Graphene–aramid nanofiber nanocomposite paper with high mechanical and electrical performance†

Jinchen Fan,[a] Zixing Shi,*[a] Ming Tian*[b] and Jie Yin[a]

A novel mechanically strong, electrically conductive nanocomposite paper based on reduced graphene oxide nanosheets and aramid nanofibers was prepared by vacuum-assisted filtration followed by reduction.

Kevlar® (poly(*para*-phenylene terephthalamide)), synthesized in solution from monomers 1,4-phenylene-diamine (*para*-phenylene-diamine) and terephthaloyl chloride in a condensation reaction, has attracted great interest in materials science and industrial applications because of its extreme physical properties and thermal performance.[1–5] Due to its liquid-crystalline behaviour, when Kevlar® is spun, the resulting typical Kevlar® fibers, also called aramid fibers, are extremely strong and stiff with a tensile strength of ~3.6 GPa and a modulus of ~90 GPa.[6,7] Typical applications of aramid fibers include combat helmets, bullet-proof vests, protective clothing, high-performance monocoque bodies for F1 racing cars and helicopter rotor blades, *etc.*[8] Kevlar® fiber has always been widely used for reinforcing composite materials, often in combination with carbon fiber and glass fiber.[9–11] In actual industrial application, Kevlar® is usually processed into Kevlar® yarns through dry-jet wet spinning. Thus, most of the research works with Kevlar® were based on the macroscopic fiber, e.g. Kevlar® yarns. The status of the macroscopic Kevlar® fiber restricts its potential application in composite materials. Inspired by Kotov's group, the dissolution of Kevlar® threads or fabrics in dimethylsulfoxide (DMSO) by controlled deprotonation with potassium hydroxide (KOH) can effectively split the bulk Kevlar® macroscale fibers into aramid nanofibers (ANFs).[12] In our previous research work, the reactive ANFs were used for the functionalization of graphene nanosheets, which resulted in novel nanofillers for polymer reinforcement.[13] Graphene nanosheets are single layer graphite sheets that consist of sp^2 carbon atoms covalently bonded in a honeycomb crystal lattice. Due to their fascinating features such as thermal conductivity, mechanical properties and enormous electronic transport properties, graphene nanosheets have aroused great interest to serve as new nanoscale building blocks to create unique macroscopic materials.[14–17] Recently, mechanically strong and electrically conductive graphene-based papers prepared by vacuum-assisted filtration have been found to be very attractive and valuable for many potential applications.[18,19] As is well-known, nanocomposite papers are often referred to as thin sheets or films made of nanomaterials such as carbon nanotubes, carbon nanofibers, nanoclays, cellulose nanofibrils and graphene nanosheets.[20–23] Cao *et al.* demonstrated that ANFs can act as high-performance polymeric building blocks and form mechanically robust ANF nanopapers.[24] Therefore, by combining ANFs and graphene nanosheets, a macroscopic nanocomposite paper with high mechanical and electrical performance can be expected.

In this communication, we report a novel nanocomposite paper based on ANFs and graphene oxide (GO) by vacuum-assisted filtration followed by reduction. The mechanical and electrical properties of nanocomposite papers have been investigated. With a synergetic effect, the combination of ANFs and graphene nanosheets can improve the mechanical performance of nanocomposite papers. The reduced graphene oxide (RGO)–ANF nanocomposite papers also exhibit good electrical conductivity.

ANFs were obtained from macroscale commercial Kevlar® 49 yarns by deprotonation of the amide groups in a solvent system of DMSO and KOH. The macroscopic-scale fibers were split into the ANFs, with a width range from 20 to 50 nm, as measured by atomic force microscopy (AFM) and transmission electron microscopy (TEM) (Fig. S3 and S4, ESI†), and yielded a stable and red dispersion of ANF–DMSO (Fig. 1b).[12] As shown in Fig. 1a, the GO–ANF nanocomposite papers were prepared by self-assembly by vacuum filtration. For the fabrication of GO–ANF composite papers, the desired amount of a GO–DMSO dispersion was slowly added into the ANF–DMSO dispersion. After stirring at 80 °C for 1 h, deionized (DI) water was poured into the reaction

[a]*School of Chemistry and Chemical Engineering & State Key Laboratory for Metal Matrix Composite Materials, Shanghai Jiao Tong University, Shanghai, 200240, People's Republic of China. E-mail: zxshi@sjtu.edu.cn; Fax: +86 21 54747445; Tel: +86 21 54743268*

[b]*State Key Laboratory of Organic-Inorganic Composites, Beijing University of Chemical Technology, Beijing, 100029, People's Republic of China. E-mail: tianm@mail.buct.edu.cn; Fax: +86 10 64434860; Tel: +86 10 64434860*

† Electronic supplementary information (ESI) available. See DOI: 10.1039/c3ra42515k
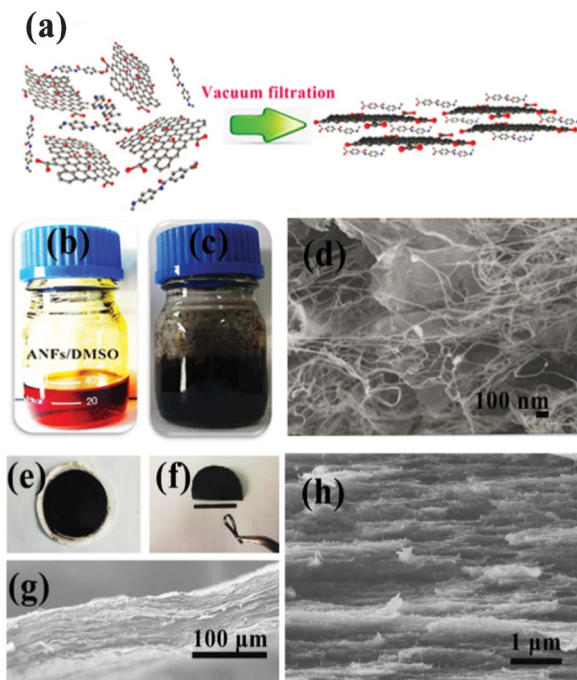
Fig. 1 (a) Schematic diagram of the fabrication of GO–ANF nanocomposite paper *via* vacuum filtration, (b) ANF–DMSO dispersion, (c) GO–ANF flocculation liquid dispersion, (d) SEM image of freeze-dried flocculated GO–ANF , (e) GO–ANF nanocomposite paper deposited on the filter film, (f) TRGO–ANF nanocomposite paper, (g) SEM image of the fracture surface of the TRGO–ANF-5 nanocomposite paper, and (h) SEM image of the fracture surface of the TRGO–ANF-5 nanocomposite paper at high resolution.

Fig. 2 (a) Typical strain–stress curves for the TRGO–ANF nanocomposite papers, (b) averaged results for the maximum tensile strength of GO, ANF and TRGO–ANF nanocomposite papers, (c) averaged results for the Young's modulus of GO, ANF and TRGO–ANF nanocomposite papers, and (d) XRD patterns of GO, RGO, Kevlar®, ANFs, ANF nanopaper and TRGO–ANF nanocomposite papers.

mixture. As observed from Fig. 1c, flocculation was generated and GO–ANF was suspended in the mixture solution.

GO has a huge surface area and its graphitized basal plane structure allows it to have strong π–π interactions with the reactive ANFs in liquid solution. From the SEM images of the freeze-dried GO–ANF flocculation dispersion, the ANFs were adhered onto the surface of GO (Fig. 1d). The layered structure of GO was also interconnected by the ANFs (Fig. S5, ESI†). Similar to free-standing graphene oxide paper, the GO–ANF nanocomposite paper was obtained *via* vacuum-assisted self-assembly (Fig. 1e). With different feed amounts, the GO–ANF nanocomposite papers are expressed as GO–ANF-*n*; where *n* represents the relative weight ratio of GO to the ANFs.

ANFs exhibit high reactivity and can act as high-performance polymeric building blocks.[24] It is worth noting that there is a gel phenomenon when the ANF–DMSO dispersion is mixed with DI water (Fig. S6, ESI†). The reactive ANF building blocks can be assembled into the gel networks of the ANFs through a deprotonation procedure after the addition of water. Due to the strong hydrogen bonding, the ANFs can form a continuous paper *via* vacuum-assisted filtration (Fig. S7, ESI†). The macroscopic ANF nanopaper has a certain mechanical performance with the tensile strength of ∼79.1 MPa. After the combination of GO and ANFs, the resulting GO–ANF nanocomposite papers exhibit good mechanical properties. For GO-based composite papers, the reduction method has an important influence on the mechanical
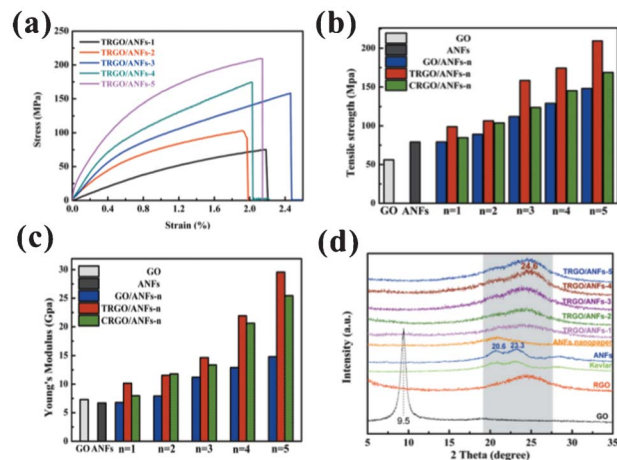
performance of the produced RGO-based composite papers.[18,19,25] Impressively, ANFs have a high thermal stability with mass loss at around 540 °C, as measured by thermogravimetric analysis (TGA) (Fig. S8, ESI†). Fig. 1f shows the obtained flexible thermally reduced graphene oxide TRGO–ANF nanocomposite paper which has been reduced by thermal annealing at 200 °C.

The strain–stress curves from tensile tests for the TRGO–ANF nanocomposite papers are illustrated in Fig. 2a. Obviously, the maximum tensile strength of TRGO–ANF-5 nanocomposite paper reaches ∼209.4 MPa, which is an increase of ∼164.7% compared to the ANF nanopaper. The maximum tensile strength of the TRGO–ANF nanocomposite paper increases with the amount of GO. From Fig. 2c, the Young's modulus of the TRGO–ANF-5 nanocomposite paper reaches ∼29.6 GPa, which is ∼4.4 times more than that of the pure ANF nanopaper. Additionally, compared to the GO and TRGO nanopapers (Fig. S9, ESI†), the introduction of ANFs can tailor the mechanical performance of the pure GO and TRGO nanopapers. The results demonstrate that the combination of ANFs and GO can yield a nanocomposite paper with a high mechanical performance. The TRGO–ANF nanocomposite paper exhibits a lamellar structure with interspersed ANFs, as observed in the SEM images of the fracture surface (Fig 1g and 1h).

The chemical reduction method was also applied for the reduction of the GO–ANF nanocomposite paper and hydriodic acid was chosen as the reducing agent. From Fig. 2b and 2c, the tensile strengths and Young's modulus of TRGO–ANF and chemically reduced GO–ANF (CRGO–ANF) nanocomposite papers both improved obviously and increased with the amount of GO. This is attributed to the enhancement of interlayer contact and interactions of the graphene nanosheets with reduction.[18,26] But for the CRGO–ANF nanocomposite paper, the mechanical performance was worse than for the TRGO–ANF nanocomposite paper. Compared to the flexible TRGO–ANF nanocomposite paper,
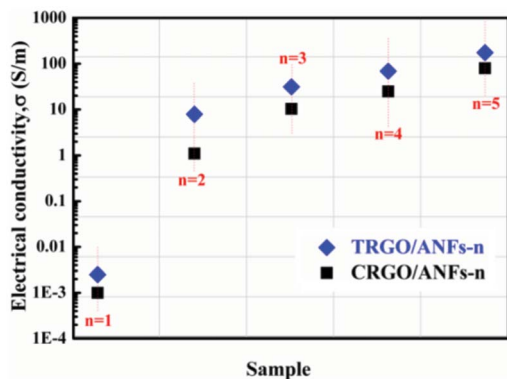
Fig. 3 Electrical conductivity of TRGO–ANF and CRGO–ANF nanocomposite papers.

the CRGO–ANF nanocomposite paper was easy to break after slight bending (Fig. S10, ESI†). In the thermal reduction method, the residual water and organic species existing between the graphene nanosheets in the GO–ANF nanocomposite paper were removed during thermal annealing, leading to a reduced distance between graphene layers. The van der Waals or π–π interactions are highly dependent on the distance between the graphene nanosheets, and significantly increase as the distance decreases. But during chemical reduction, the original layered structure of the GO–ANF nanocomposite paper is well protected after the HI acid reduction. Thus, we consider that the layered structure of the TRGO–ANF nanocomposite paper is more compact and tighter than the CRGO–ANF nanocomposite paper (Fig. S11 and S12, ESI†). As a result, thermal reduction is more beneficial for the improvement of the mechanical properties.

By combining RGO nanosheets and ANFs, the as-prepared RGO–ANF paper also exhibits a good electrical conductivity. The pure ANF papers were not electrically conductive but the introduction of the RGO nanosheets generated electrical conductivity in the RGO–ANF nanocomposite paper. From Fig. 3, the electrical conductivities of CRGO–ANF-1 and TRGO–ANF-1 nanocomposite papers are relatively low. However, as can be seen clearly, a sharp increase in the electrical conductivity was observed for CRGO–ANF-2 and TRGO–ANF-2 nanocomposite papers. This increase in the conductivity is attributed to the increased amount of RGO and the formation of an infinite network of percolated reduced graphene oxide nanosheets. The TRGO–ANF-5 and CRGO–ANF-5 nanocomposite papers showed a remarkably high electrical conductivity of ∼145.8 and 79.7 S m^{-1}, respectively.

Through strong interactions, the RGO nanosheets were interconnected by the ANFs. XRD patterns were used to characterize the layered structure of the TRGO–ANF nanocomposite paper (Fig. 2d). The diffraction pattern of the original ANFs presents two sharp peaks at $2\theta = 20.6°$ ($d = 0.43$ nm) and 23.3° ($d = 0.38$ nm), which are indexed as (110) and (200) diffractions, respectively.[27] But for the pure ANF nanopapers, the disappearance of the peak at 23.3° demonstrates the loss of crystallinity due to the hydrolysis process in the continuous ANFs nanostructured networks.[24] In the TRGO–ANF nanocomposite paper, the domi-

nant peak is at around 24.6° ($d = 0.36$ nm), which is ascribed to the graphitization due to the removal of the oxygen-containing functional groups of GO during thermal reduction.[28] This suggests that the conjugated graphene network (sp^2 carbons) with a layered structure is re-established after reduction.[29] A shoulder peak at 20.6° is attributed to the interlamellar ANFs in the TRGO–ANF nanocomposite paper. The appearance of this shoulder peak proves the introduction of ANFs, consistent with the characterization by FT-IR (Fig. S13, ESI†). With interlaminar ANFs and conjugated graphene networks, the resulting TRGO–ANF nanocomposite papers exhibit high mechanical performance and electrical conductivity. After the tensile test, the ANFs were pulled out from the layered structures of TRGO–ANF nanocomposite papers. The results reflect the interaction and synergetic effect of the ANFs and RGO nanosheets. When the nanocomposite papers were stretched, the ANFs inserted in the graphene layers participated in the stress transfer and prevented slippage between the layers. Therefore, more energy was needed to break the nanocomposite papers. Obviously, the combination of ANFs and graphene nanosheets can construct mechanically robust and electrically conductive macroscopic materials. In addition, due to the high thermal stabilities of ANFs and RGO nanosheets, the RGO–ANF nanocomposite paper also exhibits a high thermal stability.

In summary, we have presented a novel mechanically robust and electrically conductive nanocomposite paper based on aramid nanofibers and reduced graphene oxide nanosheets. The significant enhancement in the mechanical properties and electrical conductivity of the RGO–ANF nanocomposite papers can be attributed to the high aspect ratio of the graphene sheets and ANFs resulting in the formation of strong π–π stacking interactions and interlocking, together with the interfacial interactions between them. Utilizing the high thermal stability of the ANFs, the TRGO–ANF nanocomposite paper is not only very flexible, but also superior to the CRGO–ANF nanocomposite paper in its mechanical and electrical performance. We believe that the nanocomposite paper described herein could find various applications in portable and flexible electrodes, supercapacitors, electromagnetic interference (EMI) shielding devices, electromagnetic pulse (EMP) protection, etc.

References

1 M. Dobb, D. Johnson and B. Saville, *Polymer*, 1981, **22**, 960–965.
2 L. Penn and F. Larsen, *J. Appl. Polym. Sci.*, 1979, **23**, 59–73.
3 T. Sainsbury, K. Erickson, D. Okawa, C. S. Zonte, J. M. Fréchet and A. Zettl, *Chem. Mater.*, 2010, **22**, 2164–2171.
4 Y. Wang, Z. Shi and J. Yin, *Polymer*, 2011, **52**, 3661–3670.
5 I. O'Connor, H. Hayden, S. O'Connor, J. N. Coleman and Y. K. Gun'ko, *J. Phys. Chem. C*, 2009, **113**, 20184–20192.
6 T. K. Lin, S. J. Wu, J. G. Lai and S. S. Shyu, *Compos. Sci. Technol.*, 2000, **60**, 1873–1878.
7 F. Vollrath and D. P. Knight, *Nature*, 2001, **410**, 541–548.

8   D. Tanner, J. A. Fitzgerald and B. R. Phillips, *Angew. Chem., Int. Ed. Engl.*, 1989, **28**, 649–654.

9   S. R. Wu, G. S. Sheu and S. S. Shyu, *J. Appl. Polym. Sci.*, 1996, **62**, 1347–1360.

10 B. Z. Jang, *Compos. Sci. Technol.*, 1992, **44**, 333–349.

11 E. E. Magat, *Philos. Trans. R. Soc. London, Ser. A*, 1980, **294**, 463–472.

12 M. Yang, K. Cao, L. Sui, Y. Qi, J. Zhu, A. Waas, E. M. Arruda, J. Kieffer, M. D. Thouless and N. A. Kotov, *ACS Nano*, 2011, **5**, 6945–6954.

13 J. Fan, Z. Shi, L. Zhang, J. Wang and J. Yin, *Nanoscale*, 2012, **4**, 7046–7055.

14 D. A. Dikin, S. Stankovich, E. J. Zimney, R. D. Piner, G. H. B. Dommett, G. Evmenenko, S. T. Nguyen and R. S. Ruoff, *Nature*, 2007, **448**, 457–460.

15 S. Park, J. W. Suk, J. An, J. Oh, S. Lee, W. Lee, J. R. Potts, J.-H. Byun and R. S. Ruoff, *Carbon*, 2012, **50**, 4573–4578.

16 Ravikumar and K. Scott, *Chem. Commun.*, 2012, **48**, 5584–5586.

17 H. Kim, A. A. Abdala and C. W. Macosko, *Macromolecules*, 2010, **43**, 6515–6530.

18 H. Chen, M. B. Müller, K. J. Gilmore, G. G. Wallace and D. Li, *Adv. Mater.*, 2008, **20**, 3557–3561.

19 W. Huang, X. Ouyang and L. J. Lee, *ACS Nano*, 2012, **6**, 10178–10185.

20 G. Xu, Q. Zhang, W. Zhou, J. Huang and F. Wei, *Appl. Phys. A: Mater. Sci. Process.*, 2008, **92**, 531–539.

21 N. D. Luong, N. Pahimanolis, U. Hippi, J. T. Korhonen, J. Ruokolainen, L.-S. Johansson, J.-D. Nam and J. Seppala, *J. Mater. Chem.*, 2011, **21**, 13991–13998.

22 L. Yang, S. Cheng, Y. Ding, X. Zhu, Z. L. Wang and M. Liu, *Nano Lett.*, 2012, **12**, 321–325.

23 K.-L. Liang, Y.-C. Wang and J.-J. Lin, *MRS Proceedings*, 2012, **1450**, mrss12-1450-cc03-12, DOI: 10.1557/opl.2012.1373.

24 K. Cao, C. P. Siepermann, M. Yang, A. M. Waas, N. A. Kotov, M. D. Thouless and E. M. Arruda, *Adv. Funct. Mater.*, 2013, **23**, 2072–2080.

25 H. A. Becerril, J. Mao, Z. Liu, R. M. Stoltenberg, Z. Bao and Y. Chen, *ACS Nano*, 2008, **2**, 463–470.

26 P. Ajayan and O. Zhou, *Carbon Nanotubes: Synthesis, Structure, Properties and Applications*, ed. M. Dresselhaus, G. Dresselhaus and P. Avouris, Springer, Berlin, Heidelberg, 2001, pp. 391–425.

27 M. Shubha, H. V. Parimala and K. Vijayan, *J. Mater. Sci. Lett.*, 1991, **10**, 1377–1378.

28 L. Tang, Y. Wang, Y. Li, H. Feng, J. Lu and J. Li, *Adv. Funct. Mater.*, 2009, **19**, 2782–2789.

29 G. Eda, G. Fanchini and M. Chhowalla, *Nat. Nanotechnol.*, 2008, **3**, 270–274.